Simultaneous temperature and refractive index measurement of liquid using a local micro-structured fiber Bragg grating

Ye Cao (曹 晔), Yinfei Yang (杨寅飞)*, Xiufeng Yang (杨秀峰), and Zhengrong Tong (童峥嵘)

Tianjin Key Laboratory of Film Electronic and Communication Devices, School of Computer and Communication Engineering, Tianjin University of Technology, Tianjin 300384, China

**Corresponding author: yang85039890@163.com*

Received July 7, 2011; accepted September 15, 2011; posted online November 18, 2011

An alternative solution for the simultaneous measurement of temperature and refractive index is presented. A local micro-structured fiber Bragg grating (LMSFBG) is formed as the sensing head, in which a standard grating is etched by HF. According to the phase shift theory, the main spectral change of the LMSFBG is the formation of a narrow allowed band, which is strongly dependent on the etching features and the surrounding refractive index. As such, the temperature and refractive index measurements can be achieved by the shifts of the double peaks and narrow allowed band, and their fitting linearity coefficients are 0.996 and 0.994, respectively. Thus, the reflection and transmission peaks of the LMSFBG have a good linear relationship with temperature and refractive index.

OCIS codes: 060.2270, 060.2280, 060.2370, 060.2390.

doi: 10.3788/COL201210.030605.

Fiber Bragg grating (FBG) has been widely used in various industries due to its small size, ease of integration, anti-electromagnetic interference, and ability to achieve sensing information by wavelength encoding[1]. FBG also has practical applications in optical communication systems and optical sensors, such as filter devices and dual-parameter measurement sensors[2−5].

Recently, the devices based on the structure of the photonic band gap, such as phase shift grating (PSG), have attracted increasing attention. PSG has a special structure, which allows lights in different frequencies to pass through the reflection peak. In 2005, Cusano *et al.* made the first local micro-structured FBG (LMSFBG)[6], in which the FBG clad was etched partly, thus producing a non-periodic distribution structure. Therefore, a passband in the stopband came into being similar to PSG. The passband is influenced by three factors: the length of perturbation, the depth of perturbation, and surrounding refractive index (SRI). Unlike PSG, the passband can be changed by SRI. Thus, LMSFBG has a unique advantage and a higher application value in sensing and communication, because the gratings show higher sensitivity. Moreover, a special filter characteristic makes the formation of a new type of active, passive optical devices possible[7,8]. In this letter, a sensor probe is fabricated by wet chemical etching; this probe can measure the temperature and refractive indics of liquid simultaneously. In addition, it is low-cost and has a high-resolution refractive index according to the experimental results.

According to the coupled mode theory, when the FBG satisfies the phase condition, the reflected wavelength $\lambda_{\rm B}$ can be expressed as

$$\lambda_{\rm B} = 2n_{\rm eff}\Lambda, \tag{1}$$

where $n_{\rm eff}$ is the effective refractive index, and Λ is the FBG period.

However, the clad of the grating inhibits most of the evanescent waves within the core, and only a small part can pass out interacting with outside material. Therefore, FBG is not sensitive to the surrounding materials (e.g., refractive index, etc.). According to the optical waveguide theory, the effective refractive indics of guided modes vary depending on the different clad diameters. This means that, as the center of the grating is etched, the sudden change of the clad diameter leads to a change in the refractive index. Similar to the Fabry-Perot (F-P) effect, the wavelengths that meet the resonance condition of F-P cavity can pass through the grating. The passband that appears in the stopband in the reflection spectrum can be seen as the etched region of the grating, which results in phase delay[9,10]. Based on the F-P theory, the phase shift is given as

$$\Delta\Phi = \frac{4\pi}{\lambda}\Delta n_{\rm eff}({\rm SRI}, D_{\rm TH})L_{\rm TH}, \tag{2}$$

where λ is the wavelength of the light in the grating, $L_{\rm TH}$ is the length of etched area, $\Delta n_{\rm eff}$ is controlled by SRI, and $D_{\rm TH}$ is the diameter of etched clad. At the same time, more evanescent waves can spread out because of the thinner clad. As a result, the reflection and transmission peaks drift when the SRI changes.

The shifts of the reflection and transmission peaks are controlled by temperature and SRI; thus, the sensitivity coefficients are different. These coefficients can be expressed in the following matrix form:

$$\begin{bmatrix} \Delta\lambda_{\rm P} \\ \Delta\lambda_{\rm D} \end{bmatrix} = \begin{bmatrix} \frac{\partial\lambda_{\rm P}}{\partial T} & \frac{\partial\lambda_{\rm P}}{\partial n} \\ \frac{\Delta\lambda_{\rm D}}{\Delta T} & \frac{\Delta\lambda_{\rm D}}{\partial n} \end{bmatrix} \begin{bmatrix} \Delta T \\ \Delta n \end{bmatrix}, \tag{3}$$

$$\begin{bmatrix} \Delta T \\ \Delta n \end{bmatrix} = \frac{1}{D} \begin{bmatrix} \frac{\Delta\lambda_{\rm D}}{\partial n} & -\frac{\partial\lambda_{\rm P}}{\partial n} \\ -\frac{\Delta\lambda_{\rm D}}{\Delta T} & \frac{\partial\lambda_{\rm P}}{\partial T} \end{bmatrix} \begin{bmatrix} \Delta\lambda_{\rm P} \\ \Delta\lambda_{\rm D} \end{bmatrix}, \tag{4}$$

where $\Delta\lambda_{\rm P}$ is the shift of transmission peak, $\Delta\lambda_{\rm D}$ is the shift of the reflection peak, $\frac{\partial\lambda_{\rm P}}{\partial T}$ is the thermal coefficient of transmission peak, $\frac{\partial\lambda_{\rm P}}{\partial n}$ is the SRI coefficient of the transmission peak, $\frac{\Delta\lambda_{\rm D}}{\Delta {\rm T}}$ is the thermal coefficient of the

reflection peak, $\frac{\Delta\lambda_D}{\partial n}$ is the SRI coefficient of the reflection peak, ΔT represents the shift of temperature, and Δn is the shift of SRI. In addition, $D = \frac{\partial\lambda_P}{\partial T} \times \frac{\Delta\lambda_D}{\partial n} - \frac{\partial\lambda_P}{\partial n} \times \frac{\Delta\lambda_D}{\Delta T}$.

In this letter, we simulated the LMSFBG. Its schematic diagram is shown in Fig. 1. The parameters of the optical fiber for the simulation analysis were chosen according to SMF-28 standard: numerical aperture (NA) was 0.14, and refractive index difference was 0.36%. The cladding and core diameters were 125 and 8.3 μm, respectively, the grating length was 1 cm, and the grating pitch was 0.513 μm.

By substituting the parameters of the LMSFBG in Eq. (2), the phase delay at the edge of etched region can then be calculated as

$$\Delta\Phi = 0.9\pi.$$

Through the transmission matrix of Matlab, we obtained the LMSFBG spectrum shown in Fig. 2.

In the experiment, the central wavelength of FBG was 1552.760 nm, and the FBG was connected between broadband light source and an optical spectrum analyzer (OSA). The resolution of the Anritsu MS9710B OSA was 0.07 nm. The grating area can be found using an electric iron by heating the grating; the length of the grating region was 1 cm. In order to cut across the center of the grating, we used a plastic pipe with a length and radius of 0.4 and 0.2 cm, respectively. Meanwhile, the values of the L_1 and L_2 of the unpacked region are both 0.3 cm. Then, we used the needle to inject the HF acid into the plastic pipe. The HF concentration was 20%. The atmospheric pressure prevented the acid from leaking while the grating was in the plastic pipe. After 120 min of etching, we finally obtained the LMSFBG. However, the processing was not ideal because the concentration of HF acid was not always 20%; in addition, the concentration also decreased and the etched area of the LMSFBG was not exactly the same as that shown in Fig. 1. The unetched areas L_1 and L_2 also did not have the same measuring error. The LMSFBG spectrum in the experiment is shown in Fig. 3.

The etched area of the FBG shows the formation of a defect state (transmission peak) within the original grating stopband. The transmission peak is at 1 553.339 nm, whereas the double reflection peaks are at 1 553.027 and 1 553.540 nm, respectively.

Figures 2 and 3 show that there are some differences between the simulation and experimental spectra. The two reflection peaks of the simulation have almost the same amplitude; however, these have not been observed in the experiment. This phenomenon may be due

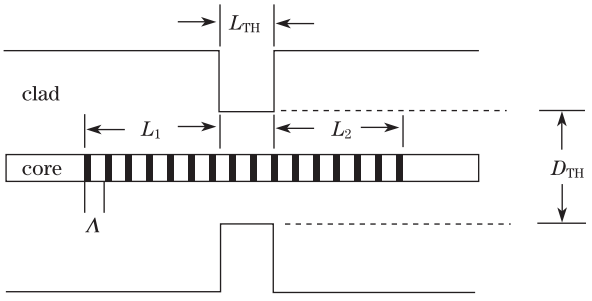

Fig. 1. Schematic diagram of the LMSFBG.

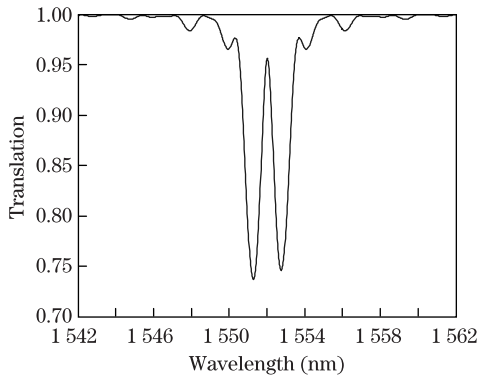

Fig. 2. Simulation transmission spectrum of the LMSFBG.

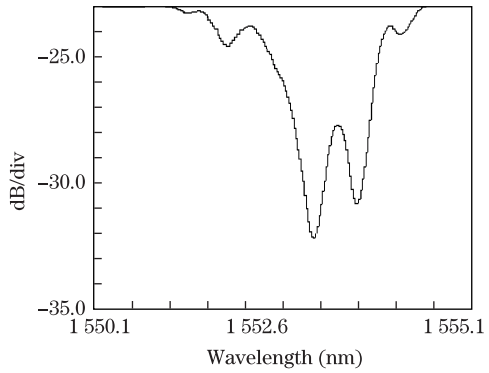

Fig. 3. Experimental transmission spectrum of the LMSFBG.

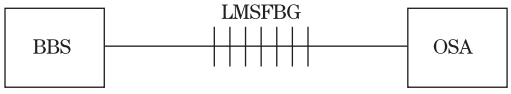

Fig. 4. Experimental setup.

to inaccurate etching, which leads to L_1 and L_2 not having the value of 0.3 cm.

The experimental setup that measures temperature and refractive index simultaneously is shown in Fig. 4. The LMSFBG was placed into the hot water (SRI=1) and then allowed to cool down while we recorded the shifts of the double reflection peaks and transmission peak every 10 nm/°C. The fitted data are shown in Fig. 5.

From the results of the fitting, the temperature-sensitive coefficient of the two reflection peaks is 0.0097 nm/°C, whereas the temperature-sensitive coefficient of the transmission peak is 0.0116 nm/°C.

In the case where the temperature is 25 °C, we used an Abbe refractometer to compound different concentrations of the NaCl solution (refractive index from 1.33 to 1.42). Then, we respectively placed the LMSFBG into the liquids and observed the wave shifts of transmission and reflection peaks in OSA.

Figure 6 shows that the LMSFBG becomes more sensitive to the surrounding material because the clad is thinner. By data fitting, the SRI-sensitive coefficients of the two reflection peaks and the transmission peaks are recorded to be about 510 and 528 nm/RIU (RIU: refractive index unit), respectively.

Substituting the coefficients into Eq. (4), we arrive at the following matrix:

$$\begin{bmatrix} \Delta T \\ \Delta n \end{bmatrix} = \frac{1}{D} \begin{bmatrix} \frac{\Delta\lambda_D}{\partial n} & -\frac{\partial\lambda_P}{\partial n} \\ -\frac{\Delta\lambda_D}{\Delta T} & \frac{\partial\lambda_P}{\partial T} \end{bmatrix} \begin{bmatrix} \Delta\lambda_P \\ \Delta\lambda_D \end{bmatrix} = \frac{1}{0.7944} \begin{bmatrix} 510 & -528 \\ -0.0097 & 0.0116 \end{bmatrix} \begin{bmatrix} \Delta\lambda_P \\ \Delta\lambda_D \end{bmatrix}. \quad (5)$$

Based on the above, the LMSFBG can measure the temperature and refractive index of the liquid simultaneously.

Then, we discuss the demodulation method applied to the LMSFBG. This method is based on the edge filtrating method and is suitable in measuring temperature and refractive index simultaneously. The system contains a 3-dB coupler, a sensing LMSFBG, two long-period gratings (LPGs), and two photo-detectors (PDs).

The schematic diagram of the demodulation system is shown in Fig. 7. The light from the BBS enters the sensing LMSFBG through a 3-dB coupler. The temperature-sensitive coefficients and the SRI-sensitive coefficients of the two reflection peaks are the same. One LPG filter was used to filtrate one reflection peak (e.g., reflection peak 1) and detect the change of temperature and SRI. The reflection peak 1 of LMSFBG drifts in the range of the rising edge of the transmission peak of LPG filter 1; the same phenomenon occurs for the transmission peak in the range of the rising edge of LPG filter 2. LPG filters 1 and 2 can filter the transmission peak and reflection peak 1 of the LMSFBG, respectively. The transmission and reflection peaks drift when temperature and refractive index change in the sensing LMSFBG area. Reflection peak 1 is demodulated in PD_1 through LPG filter 1, whereas the transmission peak is demodulated in PD_2 through LPG filter 2. PD can also detect the output optical power as well as change the signals of the

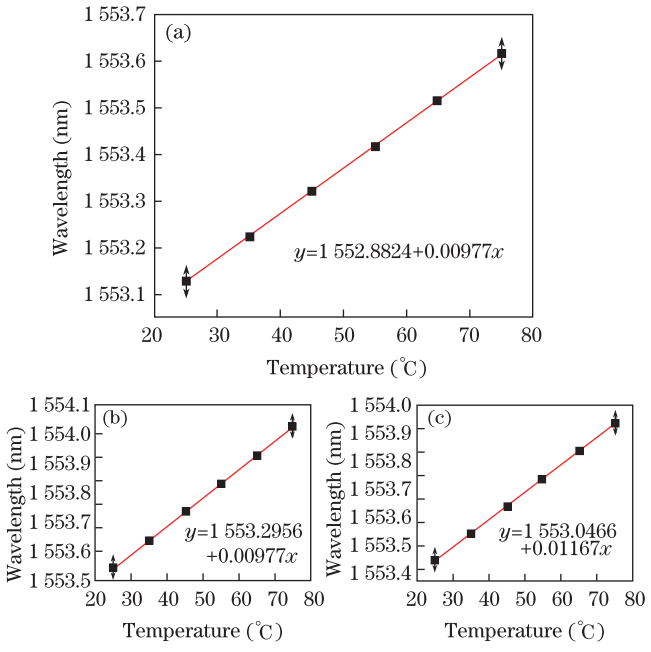

Fig. 5. Temperature response of the LMSFBG. Temperature responses of reflection peaks (a) 1 and (b) 2; (c) temperature response of transmission peak.

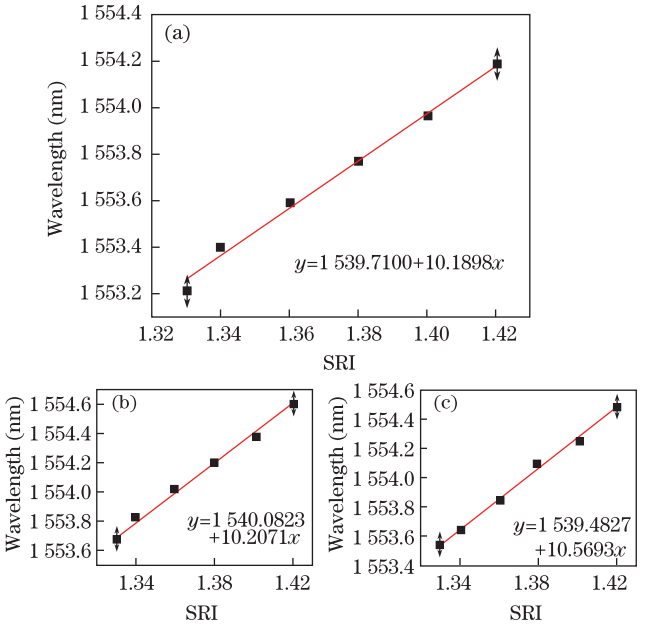

Fig. 6. SRI response of the LMSFBG. SRI responses of reflection peaks (a) 1 and (b) 2; (c) SRI response of transmission peak.

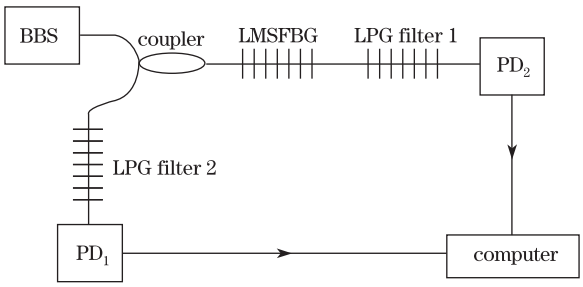

Fig. 7. Schematic diagram of the demodulation system.

temperature and refractive index of the LMSFBG sensor into electrical signals. Afterwards, the two series of data were substituted in Eq. (1) in order to determine $\Delta\lambda_P$ and $\Delta\lambda_D$. Through a matrix algorithm, the temperature and refractive index can be measured simultaneously.

In conclusion, we present a novel LMSFBG, which can measure the temperature and refractive index of liquids. By etching the center of Bragg, a passband in the FBG reflection peak appears. In waters of different temperatures, the thermal coefficients of the transmission and reflection peaks can be obtained, along with the refractive index coefficients in different concentrations of NaCl solution in the same temperature. Then, a new demodulation structure is provided to process the temperature and refractive index data. The transmission and reflection peaks have good sensitive coefficients in the temperature and refractive index. One advantage of the LMSFBG is that it is easy to make. In addition, it is convenient for practical use and has potential application for dual-parameter measurement without the package.

This work was supported by the Tianjin Natural Science Foundation (No. 11JCYBJC00100) and the National Natural Science Foundation of China (Nos.

60808004 and 61107052).

References

1. X. Cheng, W. Qiu, W. Wu, Y. Luo, X. Tian, Q. Zhang, and B. Zhu, Chin. Opt. Lett. **9,** 020602 (2011).
2. J. Yan, A. P. Zhang, L. Shao, J. Ding, and S. He, IEEE Sensor. J. **7,** 1360 (2007).
3. D. Liu, N. Q. Ngo, S. C. Tjin, and X. Dong, IEEE Photon. Technol. Lett. **19,** 1148 (2007).
4. H. Guo, G. Xiao, N. Mrad, and J. Yao, J. Lightwave Technol. **27,** 2100 (2009).
5. G. Zheng, B. Shen, J. Tan, Y. He, and X. Wang, Chin. Opt. Lett. **9,** 030501 (2011).
6. A. Cusano, D. Paladino, and A. Iadicicco, J. Lightwave Technol. **27,** 1663 (2009).
7. S. Lee, S. S. Saini, and M. Jeong, IEEE Photon. Technol. Lett. **22,** 1431 (2010).
8. A. Iadicicco, S. Campopiano, A. Cusano, M. Giordano, and A. Cusano, IEEE Photon. Technol. Lett. **17,** 1250 (2005).
9. A. Cusano, A. Iadicicco, D. Paladino, S. Campopiano, A. Cutolo, and M. Giordano, Opt. Fiber Technol. **13,** 281 (2007).
10. A. Cusano, A. Iadicicco, D. Paladino, S. Campopiano, A. Cutolo, and M. Giordano, Opt. Fiber Technol. **13,** 291 (2007).